

Identification of weak ultrasonic signals in testing of metallic materials using wavelet transform

Xianfeng Fan¹, Ming J Zuo² and Xiaodong Wang²

¹ School of Mechatronics Engineering, University of Electronic Science and Technology of China, Chengdu, Sichuan, 610054, People's Republic of China

² Department of Mechanical Engineering, University of Alberta, Edmonton, Alberta, T6G 2G8, Canada

E-mail: xianfeng.fan@gmail.com

Received 24 January 2006, in final form 13 July 2006

Published 25 September 2006

Online at stacks.iop.org/SMS/15/1531

Abstract

Non-destructive testing using ultrasonic signals has been widely employed to detect material damage and prevent accidents. A collected ultrasonic signal may be noisy and weak because of the grains in materials, incomplete contact between transducers and the mounting surface, and the long transmission path. Stationary wavelet transform has been applied together with kurtosis and universal de-noising to analyze ultrasonic signals in an attempt to identify the weak signals encountered in testing of metallic materials. The time-of-flight of signal in a metallic material is estimated by cross-correlation analysis. Application of the method is demonstrated through the ultrasonic testing of a thin steel plate with a slot.

(Some figures in this article are in colour only in the electronic version)

1. Introduction

Non-destructive testing (NDT) provides a means to test material integrity and locate degradation in structures such as ships, aircraft, reusable launch vehicles and bridges. Ultrasonic NDT has attracted the interest of researchers [1–9]. Pulse-echo is one ultrasonic technique that has attracted particular attraction [5–9]; it can measure the flight time of an ultrasonic signal from the beginning of signal transmission to the time of receipt of all echoes. In practice, the received signals may be noisy and very weak for the following reasons. First, a lot of different grains may be involved in metallic materials. Second, contact between the transducers and the mounting surface of a material is not always tight. Third, some material structures are extremely large, which results in a long transmission path for ultrasonic signals and significant signal attenuation.

Research shows that ultrasonic noise cannot be reduced by classical time-averaging or band-pass filtering techniques [6]. In addition, an ultrasonic signal transmitted into a material is usually a pulse signal that is non-stationary. Therefore, the corresponding echoes are also non-stationary. This adds to the difficulty of locating material degradation with weak

ultrasonic signals. Because Fourier transform is unable to deal with non-stationary signals, Fourier transform-based methods cannot identify weak echoes. Wavelet analysis is able to deal with non-stationary signals through time–frequency analysis and has been used in ultrasonic NDT. Serrano *et al* applied a discrete wavelet transform (DWT) together with a neural network for ultrasonic extraction of features and defect recognition in foundry pieces [7]. Draï *et al* developed a technique based on the calculation of wavelet coefficients, frequency and time-domain parameters to characterize defect echoes [8]. But issues such as the weakness and noise of ultrasonic signals are seldom addressed. Noise reduction and identification of weak ultrasonic signals are definitely helpful for location of material degradation. Rizzo and Scalea investigated ultrasonic signal de-noising using DWT through reconstruction using wavelet coefficients on each scale by setting the wavelet coefficients from other scales equal to zero [9]. Though a DWT is able to perform the time–frequency analysis and noise canceling that is necessary for the identification of weak ultrasonic signals, the DWT is not a time-invariant transform that has potential limitations. It means that even with periodic signal extension, the DWT of a

translated version of a signal x is not, in general, the translated version of the DWT of x [10]. The length N of the wavelet coefficients on each scale will become smaller at deeper wavelet decomposition levels [11]. This affects the application of the universal de-noising threshold $\sigma\sqrt{2\log(N)}$ [12] because the threshold is related to sample length N .

Pesquet and Krim proposed the stationary wavelet transform (SWT) in 1996 [10]. The SWT is similar to the DWT except that the signal is never down-sampled and the filters are different at each decomposition level. The advantage of the SWT compared with the DWT is that the SWT is time-invariant transform. The length of wavelet decomposition coefficients on each scale is equal to that of the original samples, which preserves the information redundancy. The de-noising threshold will therefore no longer be affected by wavelet transform. Cohen also agreed that restoration of the translation invariance (a desirable property lost by the classical DWT) is useful for several applications such as detection of the breakdown point and de-noising [13]. Because kurtosis is sensitive to sharp variant structures, such as impulses [14], and can measure the sudden change in the spatial variation of a signal [15], it can be employed to choose the scale where the wavelet coefficients of pulse echoes are dominant for further analysis. In order to remove the noise information from the wavelet coefficients on this selected scale, the appropriate σ of noise should be evaluated for threshold determination. Although Donoho proposed a method for estimating σ by MAD/0.6745 [16], where MAD denotes the median of the absolute deviation of a signal, this σ is only an approximate value. The true σ will be useful for improving the accuracy of the de-noising threshold. It is well known that practical ultrasonic echoes are actually the mixed signals of a pure pulse's echoes and noise. Because the echoes are not an ideal impulse signal, they only distribute on a specific scale. Therefore, the standard deviation of wavelet coefficients on some other specific scales must be close or equal to the standard deviation of the real noise wavelet coefficients. Fortunately, the SWT provides a way to obtain the standard deviation of wavelet coefficients on different scales. The appropriate standard deviation of noise wavelet coefficients may be obtained based on SWT. The de-noising threshold will be close to the true noise threshold, which can be helpful for noise reduction. Therefore, SWT should have a powerful potential to identify weak ultrasonic signals polluted by noise in metallic materials. Ultrasonic time-of-flight (TOF), which is used to estimate the location of material degradation, could be calculated through correlation analysis between the de-noised signal and the transmitted signal.

The rest of the paper is organized as follows. Stationary wavelet transform is introduced in section 2. The proposed method of combining stationary wavelet transform, kurtosis and universal de-noising method is presented in section 3 in an attempt to accurately detect the weak ultrasonic signals observed in materials testing. Experiment set-up is illustrated in section 4. Ultrasonic signals are analyzed in section 5. Conclusions are presented last.

2. Stationary wavelet transform

A wavelet $\psi(t)$ is a waveform that has a limited duration and an average value of zero on $(-\infty, \infty)$. The wavelet family can

be represented by

$$\psi_{a,b} = |a|^{-1/2}\psi\left(\frac{t-b}{a}\right), \quad (1)$$

where a and b represent the dilation and time parameters of the wavelet [17]. $a > 0$, $b \in R$. $\psi_{a,b}$ means a wavelet which is formed from a mother wavelet function $\psi(t)$ through rescaling and shifting. Continuous wavelet transform (CWT) of the signal $x(t)$ can be given by

$$w_{a,b} = \langle x(t), \bar{\psi}_{a,b} \rangle = |a|^{-1/2} \int x(t)\bar{\psi}\left(\frac{t-b}{a}\right) dt, \quad (2)$$

where $w_{a,b}(t)$ denotes wavelet transform coefficients [17], $x(t)$ is a source signal, $\langle \cdot, \cdot \rangle$ represents the inner product operation and $\bar{\psi}$ denotes the complex conjugate. In application, time-scale parameters (b, a) are sampled so that the signal could be represented by wavelet coefficients in an economical manner through the definitions of $a = 2^j$ and $b = k2^j$. Equation (1) becomes [18]

$$\psi_{j,k} = 2^{-j/2}\psi(2^{-j}t - k), \quad (3)$$

where j and k are arbitrary integers. Wavelet coefficients will then be obtained correspondingly by

$$w_{j,k} = \langle x(t), \bar{\psi}_{j,k} \rangle = 2^{-j/2} \int x(t)\bar{\psi}(2^{-j}t - k) dt, \quad (4)$$

which is called the DWT [19]. Mallat proposed a multi-resolution pyramidal algorithm for fast DWT by [11]

$$\langle x(t), \phi_{j,k} \rangle = \sum_k \langle x(t), \phi_{j-1,k} \rangle g(k - 2n), \quad (5)$$

$$\langle x(t), \psi_{j,k} \rangle = \sum_k \langle x(t), \phi_{j-1,k} \rangle h(k - 2n), \quad (6)$$

where $\phi_{j,k}$ is a scaling function. $g(k)$ and $h(k)$ are the impulse response of low pass and high pass filters, called quadrature mirror filters (QMFs) [20].

Let us consider a signal $x(n)$ and $c_{j-1,k} = \langle x(n), \phi_{j-1,k} \rangle$. n is an arbitrary integer. According to equations (5) and (6), the DWT of signal $x(n)$ can be obtained by

$$c_{0,n} = x(n), \quad (7)$$

$$c_{j,n} = \sum_k c_{j-1,k} g(k - 2n), \quad (8)$$

$$w_{j,n} = \sum_k c_{j-1,k} h(k - 2n). \quad (9)$$

$c_{j,n}$ and $w_{j,n}$ are discrete scaling coefficients and wavelet coefficients. They represent the approximation and discrete details of signal $x(n)$ at resolution 2^j , respectively. In equations (8) and (9), a down-sampling algorithm, which keeps one point out of two, is used to perform the transform. The whole length of the signal $x(n)$ will reduce by half after each transform until the length of the wavelet coefficients on the first scale is equal to 1. Therefore, the time-invariance property cannot be guaranteed.

Corresponding to the down-sampling algorithm, the up-sampling algorithm can be defined as $f(2n) = f(n)$ and $f(2n + 1) = 0$. SWT is the extension of DWT [10]. The

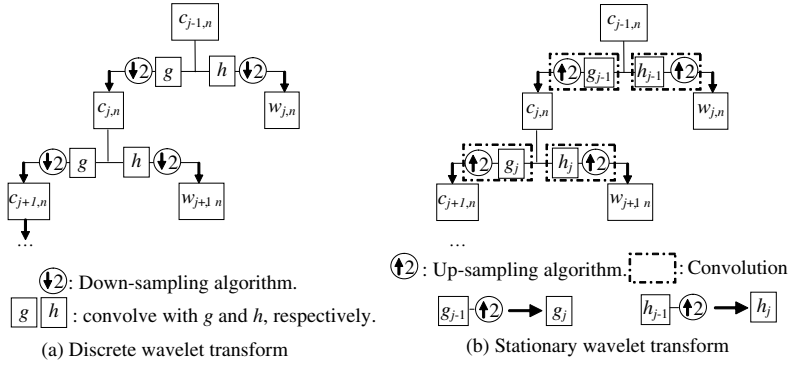


Figure 1. Discrete wavelet transform and stationary wavelet transform.

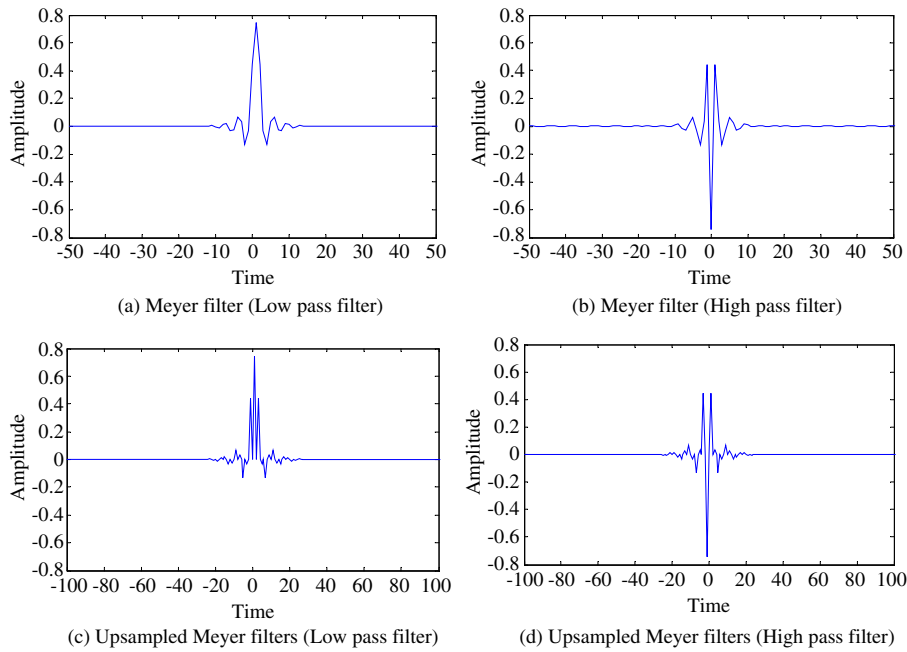


Figure 2. Scaling function and wavelet function of the Meyer wavelet.

basic idea is to modify the quadrature mirror filters through the up-sampling algorithm before performing the filter convolution on each scale in order to keep the redundancy of wavelet transforms. The key is to modify filters by the insertion of zeros. Therefore, equations (8) and (9) can be revised as

$$c_{j,n} = \sum_l c_{j-1,n+2^{j-1}l} g(l), \quad (10)$$

$$w_{j,n} = \sum_l c_{j-1,n+2^{j-1}l} h(l), \quad (11)$$

respectively [21], where l is an arbitrary integer. SWT coefficients $\{swc_{j,n} | \hat{j} = 1, 2, \dots, J + 1\}$ consist of $c_{J,n}, w_{J,n}, w_{J-1,n}, \dots, w_{1,n}$ at decomposition level J .

The difference between DWT and SWT is illustrated in figure 1. Figure 1(a) shows the Mallat pyramid algorithm [11]. The filters g and h are not varied during the DWT on each scale. Down-sampling is performed on the transform coefficients. Figure 1(b) presents the algorithm of the

SWT [10]. The filters g and h are up-sampled before performing the next transform. g_j and h_j represent the filters used at resolution 2^j . A restriction should be satisfied for the application of the SWT. That is, the length of the signal should be divisible by 2^J where J is the maximum decomposition level that we choose. When the high-pass and low-pass filters are applied to a signal, the two new sequences have the same length as the original sequence, which remain the time-invariance property of wavelet coefficients. Therefore, the SWT coefficients of a delayed signal are just a time-shifted version of those of the original one [22].

The Meyer wavelet, a biorthogonal wavelet, is available to be used in discrete wavelet transform [23]. In order to illustrate the modification of filters, the Meyer scaling function (low pass filter), the wavelet function (high pass filter) and their corresponding up-sampled filters are shown in figures 2(a)–(d), respectively. Comparing figures 2(a) and (b) with 2(c) and (d), respectively, we can notice that the filters in figures 2(a) and (b) are modified and their length is extended.

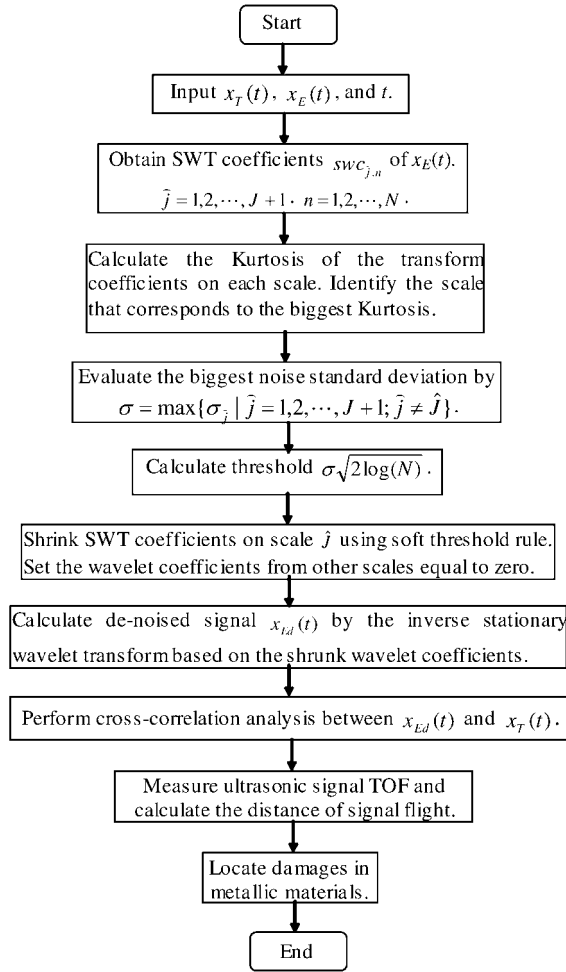


Figure 3. A flow chart of the proposed method.

3. The proposed method

We present method for identification of weak ultrasonic signals based on the following assumption. The frequency components of all reflection, refraction and scattered echoes are the same if a pulse signal is transmitted into a metallic material. This means that all the received signals have the same frequency. In practice, the received echoes only contain pulse echoes and noise. The echoes are not ideal impulse signals: they only distribute in a specific frequency band that corresponds to a specific scale instead of the entire frequency domain.

Figure 3 shows a flow chart of the proposed method. $x_T(t)$ is a transmitted signal. SWT is used to decompose the received signal $x_E(t)$ into multi-transform coefficient sets. Each coefficient set locates in a specific frequency band (t is time). Taking figure 4 as an example, if a raw signal is decomposed to the J th level, we may obtain $(J + 1)$ data sets: $\hat{j} = 1, 2, \dots, J + 1$. N represents the length of the raw signal, as well as the length of the wavelet coefficients in each data set. n represents the n th point in each data set. $swc_{\hat{j},n}$ represent the SWT coefficients on the scale \hat{j} .

After obtaining SWT coefficients, noise should be removed. Kurtosis defined by

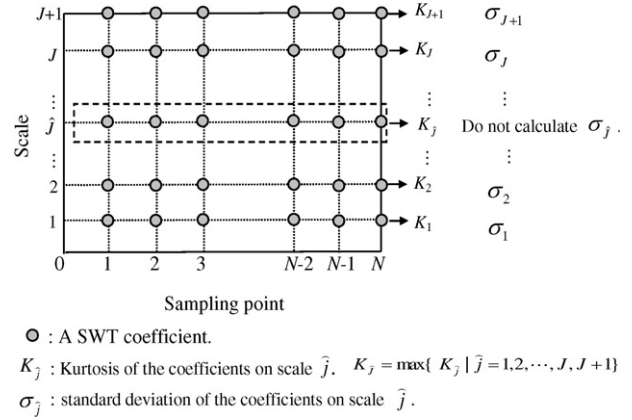


Figure 4. Kurtosis and standard deviation of SWT coefficients.

$$\text{kurtosis} = \frac{\sum_i (x_i - \bar{x})^4 / N}{(\sum_i (x_i - \bar{x})^2 / N)^2} \quad (12)$$

is used in this paper as a criterion for noise removal because it has a higher value for a sharp variant structure and a lower value for a non-sharp variant structure, such as noise which distributes in the entire time–frequency plane [14]: x is the sampled time series, x_i is the i th sample in x , \bar{x} is the mean and N is the length of x . In figure 4, for the coefficients on each scale, we calculate kurtosis and select the scale denoted by \hat{J} that corresponds to the maximum kurtosis $K_{\hat{J}}$. Then, all the coefficients except that on scale \hat{J} will be set to zero. That means, if $\hat{j} \neq \hat{J}$, then we let $\overline{swc_{\hat{j},n}} = 0$. $\overline{swc_{\hat{j},n}}$ represent the zeroed $swc_{\hat{j},k}$ when $\hat{j} \neq \hat{J}$.

But noise still exists in the remaining coefficients on scale \hat{J} . Because soft-thresholding has advantages such as achieving a near-optimal minimax rate, smaller risk and visual improvement [21], it can be used to shrink the coefficients on the scale \hat{J} . The soft-threshold rule is defined by [12]

$$\overline{swc_{\hat{j},n}} = \begin{cases} \text{sgn}(swc_{\hat{j},n})(|swc_{\hat{j},n}| - \text{th}) & |swc_{\hat{j},n}| \geq \text{th} \\ 0 & |swc_{\hat{j},n}| < \text{th}, \end{cases} \quad (13)$$

where $\overline{swc_{\hat{j},n}}$ and $swc_{\hat{j},k}$ represent shrunk SWT coefficients and original SWT coefficients on the scale \hat{J} , respectively, th represents the threshold, $\text{th} = \sigma\sqrt{2\log(N)}$ and $\text{sgn}(\cdot)$ is a signum function. Because we assume that all the echoes have same frequency, the coefficients of echoes will locate in a specific frequency band, which corresponds to a scale. The coefficients on other scales should be close to the coefficients of noise. In order to completely remove noise, we let $\sigma = \max\{\sigma_{\hat{j}} | \hat{j} = 1, 2, \dots, J + 1; \hat{j} \neq \hat{J}\}$. Here, standard deviations $\{\sigma_{\hat{j}} | \hat{j} = 1, 2, \dots, J + 1; \hat{j} \neq \hat{J}\}$ are calculated using the coefficients on all scales except \hat{J} before setting $swc_{\hat{j},n} = 0$ (see figure 4). Through the inverse stationary wavelet transform based on these shrunk SWT coefficients $\overline{swc_{\hat{j},n}}$, $\hat{j} = 1, 2, \dots, \hat{J}, \dots, J + 1$, we can reconstruct the de-noised signal.

Correlation analysis is a powerful tool for the measurement of coherence between signals. The peaks as a result of

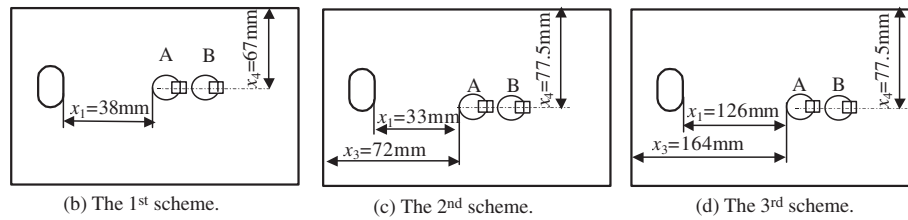
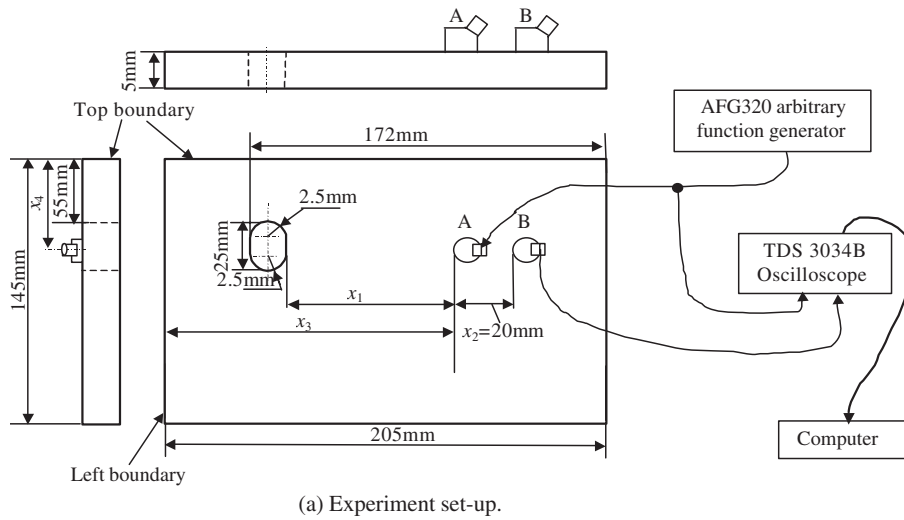


Figure 5. Experimental set-up.

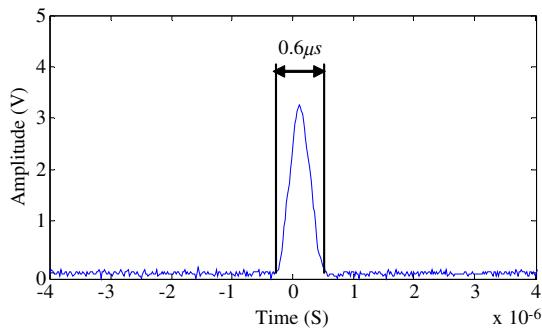


Figure 6. A pulse signal.

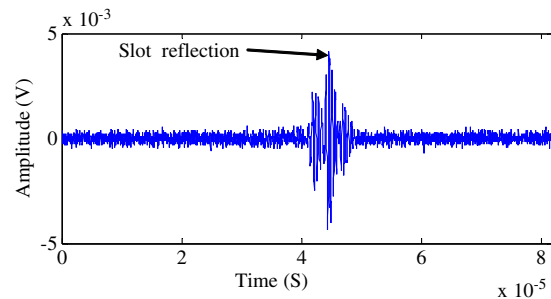


Figure 7. The raw signal received for the first scheme of the experiment.

cross-correlation between two signals indicate the time of flight between them. This is particularly useful for a transportation delay. Let $x(t)$ and $y(t)$ be two different random time series, the cross-correlation between them could be represented by [24]

$$R_{xy}(t) = \int_{-\infty}^{\infty} x(\tau)y(\tau-t) d\tau = \int_{-\infty}^{\infty} x(\tau+t)y(\tau) d\tau. \quad (14)$$

This equation indicates that there is a time $t = \tau$ at which the absolute value of the cross-correlation function is equal to or greater than at any other time. The appearance time of a larger peak, which is the TOF of ultrasonic signal, indicates a resemblance between the received signal and the transmitted signal [25]. The distance between an ultrasonic sensor and the damage in a metallic material could be calculated according to the TOF and the speed of transmission in the material.

4. Experimental set-up

The experiments used to demonstrate the application of the proposed method were conducted with an ultrasonic pulser/receiver system on a thin 347 stainless steel plate with a slot. The experimental set-up is shown in figure 5(a). The slot in the plate was generated to simulate damage to a metallic material. Because shear wave transducers are suitable for measuring the relative distance of the object from the mounting position of the transducers [26] and a shear vertical (SV) wave at 45° incidence is optimal for the inspection of crack-like damage [27], they are adopted in this experiment. The velocity of the plane shear wave is 3100 m s⁻¹. Two 2.25 MHz beam transducers (0.5 in × 1.0 in), A and B, with 45° angle wedges are tandem mounted on the same side of the slot to respectively launch and receive ultrasonic signals. An ultrasonic couplant of type XD-740 (General Electric) is

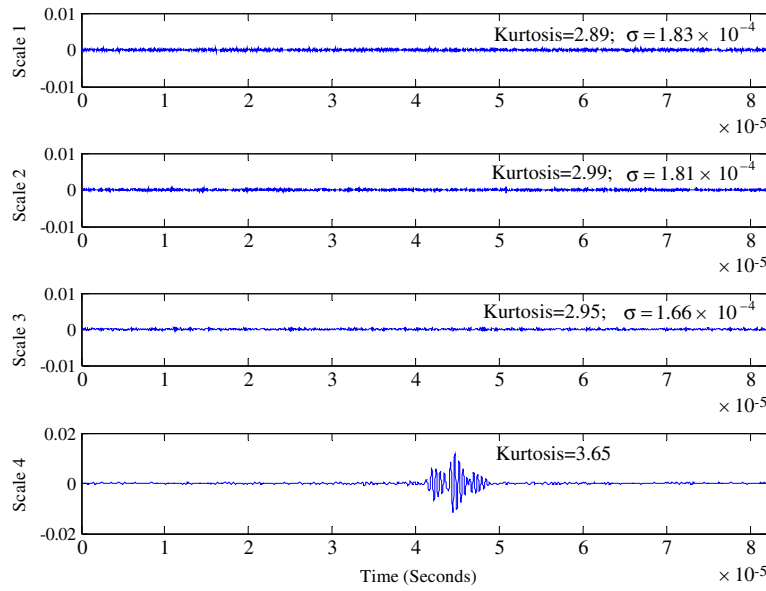


Figure 8. SWT of the signal received for the first scheme of the experiment.

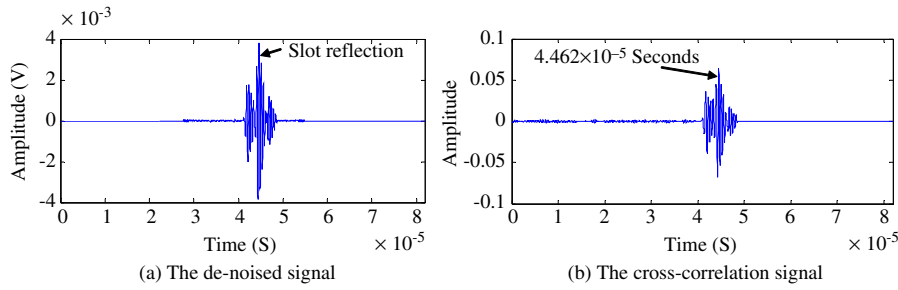


Figure 9. De-noised signal and TOF detection of the signal received for the first scheme of the experiment.

used between the transducers and the surface of the plate. x_1 represents the distance between the slot and transducer A and x_2 represents the distance between transducers A and B ($x_2 = 20$ mm). x_3 denotes the distance between the left boundary of the plate and transducer A. x_4 denotes the distance from the top boundary of the plate to both transducers A and B. Let D represent the distance of ultrasonic signal flight. \hat{x} represents the distance between transducer A and the plane of reflection. The plane of reflection may be the slot or the left boundary of the plate. Because the transmitted signal has 45° incidence, we have the following relationship:

$$D = (2\hat{x} + x_2) / \sin 45^\circ. \quad (15)$$

Both transmitted and received signals are shown by a TDS 3034B oscilloscope and saved by a computer. The experiment contains three schedules, shown in figures 5(b)–(d), respectively. Different distance between transducer and slot and different couplant conditions are achieved in order to simulate ultrasonic signals, including weak and noisy ones. In addition, we expect to identify the echoes reflected by both the slot and the left boundary simultaneously in figures 5(c) and (d).

A pulse signal generated by the AFG 320 arbitrary function generator is used as the transmitted signal, shown

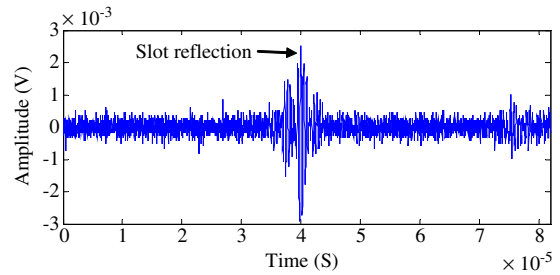


Figure 10. The raw signal received for the second scheme of the experiment.

in figure 6. The pulse duration is $0.6 \mu s$ corresponding to 1.67 MHz.

5. Ultrasonic signal analysis

Ultrasonic signals are analyzed in order to demonstrate the application of the proposed method. A Meyer wavelet is employed for SWT in this study because the shape of a Meyer wavelet is similar to that of the created pulse signal. The decomposition level of the SWT is chosen as $J = 3$.

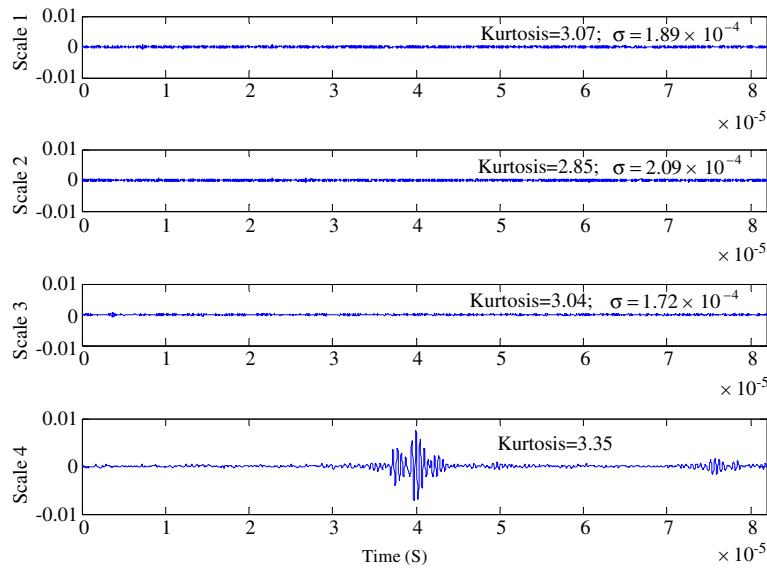


Figure 11. SWT of the signal received for the second scheme of the experiment.

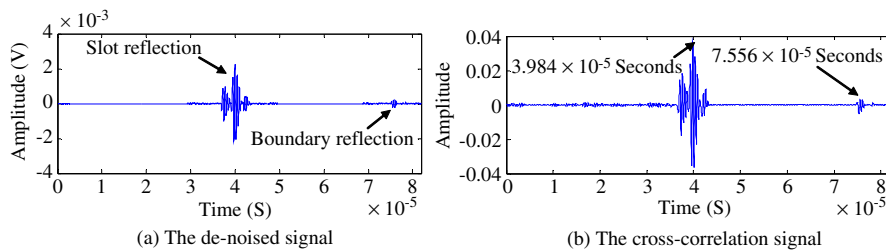


Figure 12. De-noised signal and TOF detection of the signal received for the second scheme of the experiment.

In the first experimental scheme, transducers A and B are mounted as in figure 5(b) ($x_4 = 67$ mm). The pulse response from the slot plane is expected to be received by transducer B. Figures 7 and 8 show the raw echo signal received and its SWT coefficients, respectively. The coefficient set on the fourth scale has the biggest kurtosis, $K_4 = 3.65$. The standard variances of the coefficient sets on the first–third scale are calculated. The biggest, $\sigma = 1.83 \times 10^{-4}$, is chosen to calculate the de-noising threshold. The de-noised signal is shown in figure 9(a). The cross-correlation signal between the transmitted signal and the de-noised echo signal is presented in figure 9(b). We can extract the TOF of 4.462×10^{-5} s in figure 9(b). According to equation (15), we evaluate $\hat{x} = 38.9$ mm that is close to x_1 in figure 5(b). Therefore, the location of the slot can be detected.

In the second experimental scheme, transducers A and B are put as in figure 5(c). Pulse responses from both the slot plane and the plate's left boundary are expected to be in the signal received by transducer B. Figures 10 and 11 show the raw echo signal and its SWT coefficients, respectively. Only the reflection of the slot can be found in the raw signal. The coefficient set on scale 4 has the biggest kurtosis, 3.35. The biggest $\sigma = 2.09 \times 10^{-4}$ is chosen to calculate the de-noising threshold. The de-noised signal and the cross-correlation signal are presented in figures 12(a) and (b), respectively. Reflections of both the slot and the boundary are visible in figure 12(a). Two TOFs, 3.984×10^{-5} and 7.556×10^{-5} s, can

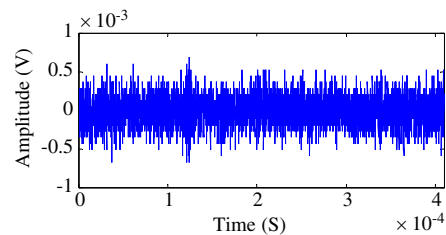


Figure 13. The raw signal received for the third scheme of the experiment.

be identified in figure 12(b). We can calculate that $\hat{x} = 33.7$ and 72.8 mm. They are close to $x_1 = 33$ mm and $x_3 = 72$ mm, respectively. Therefore, the proposed method can identify both the strong and weak ultrasonic signals that make it easy to locate the slot and the left boundary of the plate.

In the third experimental scheme, transducers A and B are mounted as figure 5(d). In order to simulate weak ultrasonic signals, x_1 and x_3 are increased and less couplant is used compared with that in the first and second experimental schemes. Pulse responses from both the slot plane and the plate's left boundary are expected to be identified from the signal received by transducer B. Figure 13 shows the raw echo signal. There are no obvious pulses existing in the figure.

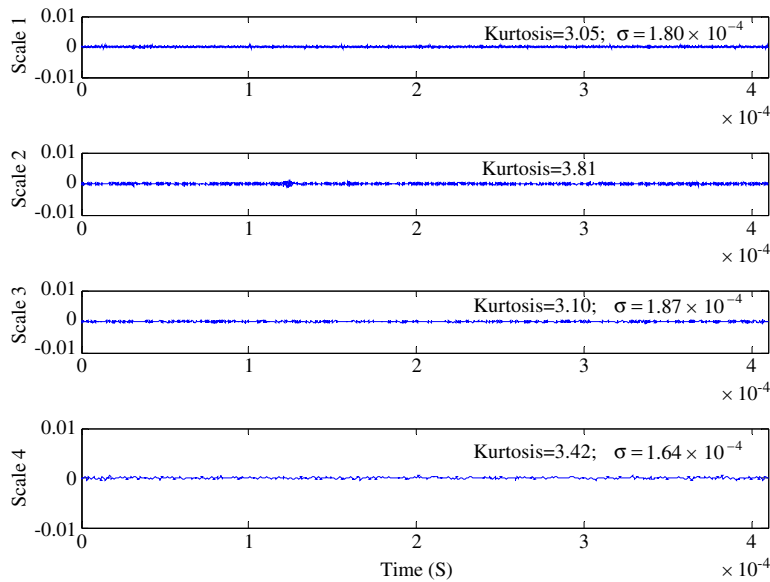


Figure 14. SWT of the signal received for the third scheme of the experiment.

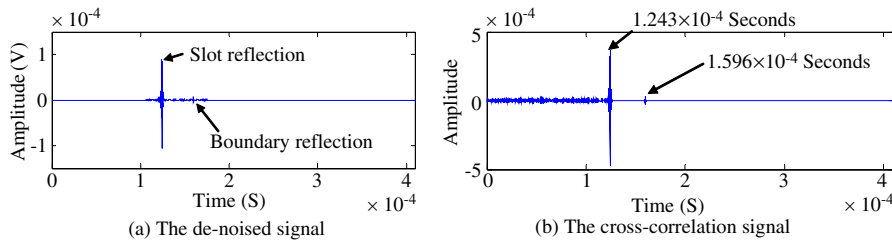


Figure 15. De-noised signal and TOF detection of the signal received for the third scheme of the experiment.

Figure 14 gives the SWT coefficients. The coefficient set on scale 2 has the biggest kurtosis, 3.81. The biggest $\sigma = 1.87 \times 10^{-4}$ is chosen for de-noising. The de-noised signal and cross-correlation signal between the transmitted signal and the de-noised echo signal are presented in figures 15(a) and (b), respectively. The TOFs 1.243×10^{-4} and 1.596×10^{-4} s can be measured in figure 15(b). The flight distances may be calculated as $\hat{x} = 126.2$ and 164.9 mm, which are close to $x_1 = 126$ mm and $x_3 = 164$ mm, respectively. Therefore, we can locate the slot and the left boundary of the plate through the identification of weak ultrasonic signals.

6. Conclusions

The identification of weak ultrasonic signals will help to improve the capability for testing material integrity and locating degradation in materials. An method of identification of weak ultrasonic signals based on stationary wavelet transform, kurtosis and cross-correlation analysis is proposed in this paper. The following conclusions are obtained. A Meyer wavelet is available to extract pulse responses from ultrasonic signals. The maximum standard variance of stationary wavelet transform coefficients on the scale that does not correspond to the maximum kurtosis can be used for evaluation of the noise threshold. Kurtosis can be used to select the scale where

the SWT coefficients should be retained. Weak ultrasonic signals can be identified by the proposed method based on a combination of SWT, kurtosis and the soft-threshold rule for noise canceling. Cross-correlation between the transmitted signal and the de-noised signal can disclose the TOF very well for estimating damage locations. The application of the proposed method is demonstrated by experiments.

Acknowledgments

This research is supported by the Natural Science and Engineering Research Council of Canada and partially supported by the Open Fund of the State Key Laboratory of Vibration, Shock and Noise of Shanghai Jiaotong University under grant VSN-2006-03. We thank Mr J Zhang and Mr C C Ng for their assistance in data collection and the anonymous referees for their many constructive comments.

References

- [1] Mak D K 1985 Ultrasonic methods for measuring crack location, crack height and crack angle *Ultrasonics* **23** 223–6
- [2] Paradis L, Serruys Y and Saglio R 1986 Time-of-flight method for crack evaluation using focused ultrasonic probes *Mater. Eval.* **44** 568–70

- [3] Vanlanduit S, Guillaume P and Van Der Linden G 2003 On-line monitoring of fatigue cracks using ultrasonic surface waves *NDT & E Int.* **36** 601–7
- [4] Beller M 2003 A new generation—Ultrasonic in-line inspection tools for the metal loss and crack inspection of pipelines *Oil Gas Eur. Mag.* **29** 88–9
- [5] Akanda M A S and Saka M 2004 Relationship between closure stress of small fatigue crack and ultrasonic response *J. Nondestruct. Eval.* **23** 37–47
- [6] Lázaro J C, San E J L, Ramos A and Fernández-Marrón J L 2002 Influence of thresholding procedures in ultrasonic grain noise reduction using wavelets *Ultrasonics* **40** 263–7
- [7] Serrano I, Lázaro A and Oria J P 1999 Ultrasonic inspection of foundry pieces applying wavelet transform analysis *Proc. 1999 IEEE Int. Symp. of Intelligent Control/Intelligent Systems and Semiotics (Cambridge, MA, Sept. 1999)* pp 375–80
- [8] Draï R, Khelil M and Benchaala A 2002 Time frequency and wavelet transform applied to selected problems in ultrasonics NDE *NDT & E Int.* **35** 567–72
- [9] Rizzo P and Scalea F L 2005 Ultrasonic inspection of multi-wire steel strands with the aid of the wavelet transform *Smart Mater. Struct.* **14** 685–95
- [10] Pesquet J C H and Krim H C 1996 Time-invariant orthonormal wavelet representations *IEEE Trans. Signal Process.* **44** 1964–70
- [11] Mallat S 1989 A theory for multiresolution signal decomposition: the wavelet representation *IEEE Trans. Pattern Anal. Mach. Intell.* **11** 674–93
- [12] Donoho D L 1995 De-noising by soft-thresholding *IEEE Trans. Inform. Theory* **41** 613–27
- [13] Cohen A 1995 *Wavelets and Multiscale Signal Processing* (London: Chapman and Hall)
- [14] Qu L and He Z 1986 *Mechanical Diagnostics* (Shanghai: Shanghai Science and Technology Press)
- [15] Hadjileontiadis L J, Douka E and Trochidis A 2005 Crack detection in beams using kurtosis *Comput. Struct.* **83** 909–19
- [16] Donoho D L and Johnstone I M 1994 Ideal spatial adaptation by wavelet shrinkage *Biometrika* **81** 425–55
- [17] Goupillaud P, Grossmann A and Morlet J 1984 Cycle-octave and related transforms in seismic signal analysis *Geoexploration* **23** 85–102
- [18] Rioul O and Vetterli M 1991 Wavelets and signal processing *IEEE Signal Process. Mag.* **8** 14–38
- [19] Shensa M 1992 The discrete wavelet transform: wedding the trous and mallat algorithms *IEEE Trans. Signal Process.* **40** 2464–82
- [20] Vaidyanathan P P 1993 *Multirate Systems and Filter Banks* (Englewood Cliffs, NJ: Prentice-Hall)
- [21] Wang X H, Istepanian R S H and Song Y H 2003 Microarray image enhancement by denoising using stationary wavelet transform *IEEE Trans. Nanobiosci.* **2** 184–9
- [22] Ye H, Wang G and Ding S X 2004 A new parity space approach for fault detection based on stationary wavelet transform *IEEE Trans. Autom. Control* **49** 281–7
- [23] Shen X A and Walter G G 2002 Meyer wavelet regularization *Numer. Funct. Anal. Optim.* **23** 195–215
- [24] Sedat S S 2005 A cross-correlation technique as a system evaluation tool; application to blood flow measurement in extra-corporeal circuits flow *Meas. Instrum.* **16** 27–34
- [25] Poularikas A D and Seely S 1988 *Elements of Signals and Systems* (Boston, MA: PWS-KENT)
- [26] Yang W X, Hill J B and Seymour M D 2004 A contribution to the applicability of complex wavelet analysis of ultrasonic signals *NDT & E Int.* **37** 497–504
- [27] Pecorari C 2005 A note on the sensitivity of SV wave scattering to surface-breaking cracks *Ultrasonics* **43** 508–11